Journal of Photochemistry and Photobiology A: Chemistry 208 (2009) 195–202

Contents lists available at ScienceDirect

Journal of Photochemistry and Photobiology A: Chemistry

journal homepage: www.elsevier.com/locate/jphotochem

Synthesis and photophysics of colloidal ZnS/PbS/ZnS nanocomposites—An analysis of dynamics of charge carriers

Anil Kumar*, Anshuman Jakhmola, Vidhi Chaudhary

Department of Chemistry and Centre of Nanotechnology, Indian Institute of Technology Roorkee, Roorkee 247667, Uttaranchal, India

ARTICLE INFO

Article history:
Received 5 January 2009
Received in revised form 29 June 2009
Accepted 15 September 2009
Available online 20 September 2009

Keywords:
Photophysics
Fluorescence
Time-resolved emission
Nanocomposite
Semiconductor
Colloid

ABSTRACT

The deposition of Q-ZnS layer as shell at the interface of Q-ZnS/PbS produces ZnS/PbS/ZnS nanocomposite. The electronic properties of the nanocomposite have been examined as a function of thickness of ZnS shell and in the presence of excess [Zn^{2+}]. The monolayer of ZnS shell red shifts the onset of absorption of precursor ZnS/PbS accompanied with an increase in absorption coefficient in the wavelength range of 200–600 nm having an excitonic absorption at 280 nm. These particles display relatively intense blue-shifted 505 nm (2.45 eV) emission associated with a tremendous enhancement of fluorescence lifetime to 150 ns from 5.5 ns, observed for precursor ZnS/PbS. The addition of Zn^{2+} further improves the charge separation in this system. These electronic changes are understood by the distribution of traps of varied energy (160–365 meV) at the interface and confinement of e^-–h^+ on the entire heterostructure.

1. Introduction

In recent years an enormous interest has aroused in PbS-based nanomaterials because of their unique optical and emission properties, which have tremendous applications in lasers [1], light emitting devices [2,3], detectors [4], solar cells [5,6], single electron devices [1], optical switches [7], telecommunication [8,9], and biological imaging [10]. In order to modify the surface and electronic properties, these particles have been synthesized in a variety of organized media such as surfactants [11,12], polymers [13,14], micelles [15,16], vesicles [17], zeolites [18,19], Langmuir–Blodgett films [20] and glasses [21,22]. The exchange of cation(s) has also been used to synthesize coupled nanoparticles of varied size and shape [23,24]. Interfacing of core semiconductor particles with a wider bandgap material as shell has been considered as another important strategy to control the surface properties for photonic applications [25,26]. In our previous work PbS-based core–shell type particles, ZnS/PbS and PbS/ZnS, were synthesized and their photophysics was monitored under different experimental conditions [27].

Several investigations have focused on forming the quantum dots quantum well (QDQW) by sandwiching the low bandgap material in the well between the layers of quantum dots of higher bandgap material *viz.* ZnS/CdS/ZnS [28,29], CdS/HgS/CdS [30], ZnS/CdSe/ZnS [31]. A number of interesting electronic features have been observed in these studies. It is still a challenging task to synthesize and understand such nanocomposites thoroughly in terms of interaction between its different components and to examine dynamics of charge carriers under irradiation for their better utilization as photonic materials.

In the present work ZnS/PbS/ZnS nanoheterostructure has been synthesized by interfacing of ZnS on ZnS/PbS particles. A coating of the monolayer of ZnS on ZnS/PbS changes their optical behavior and improves significantly the fluorescing efficiency. Photophysics and relaxation charge dynamics in these systems have been investigated under different experimental conditions. Interestingly, relaxation kinetics reveals the energy dependence decay of fluorescence suggesting the delocalization of traps of varied energy at their interface. The role of interface in these particles is discussed.

2. Materials and methods

2.1. Materials

Lead acetate and sodium hexametaphosphate (Qualigens); anhydrous zinc acetate (Fluka); sodium hydroxide (BDH); carbon coated copper grid (Polaron), nitrogen gas and oxygen gas (Grade 1, purity > 99.99%) (Sigma) were used. All chemicals were of analytical grade and were used as received.

* Corresponding author. Tel.: +91 1332 285799; fax: +91 1332 273560.
E-mail address: anilkfcy@iitr.ernet.in (A. Kumar).

1010-6030/$ – see front matter © 2009 Elsevier B.V. All rights reserved.
doi:10.1016/j.jphotochem.2009.09.015

2.2. Equipment

Electronic spectra were recorded on a Shimadzu UV2100S spectrophotometer. Emission measurements were made on a Shimadzu RF-5301PC spectrofluorophotometer. Electron microscopy was performed on a Fei-Philips Morgagni 268D Digital TEM with image analysis system having variable magnifications up to 280,000×. X-ray diffraction patterns were recorded on a Philips DW 1140/90 X-ray diffractometer using Cu Kα line of the X-ray source. The fluorescence lifetime in nanosecond time domain was recorded on a Horiba Jobin Yvon 'FluoroCube Fluorescence Lifetime System' equipped with NanoLEDs and LDs. With these systems the emitted photons were detected by using a Hamamatsu (R 3809 U) photomultiplier and thermoelectrically cooled TBX-04-D detector. Hamamatsu photomultiplier was used for the detection of fluorescence. Photolysis of different semiconductor systems were carried out on an Oriel photolysis assembly equipped with stand alone ignitor and a 200W mercury–xenon lamp. Solid samples were prepared by removing water from the colloidal solution on a Buchi Rotavapor RIIH.

For time-resolved fluorescence measurements the average lifetime (<τ>) was calculated using the relationship given below by James et al. [32]:

$$<\tau>=\frac{\sum_{i=1}^{3} b_i \tau_i^2}{\sum_{i=1}^{3} b_i \tau_i}$$

where b_i is the pre-exponential factor corresponding to the respective lifetime component τ_i. From the values of τ for different components, the depth of traps has been estimated by using Arrhenius equation in which the activation energy has been taken as the trap depth [33]. The goodness-of-fit was determined by evaluating χ^2 from a plot of the weighted residuals and auto-correlation functions.

2.3. Synthesis of ZnS/PbS/ZnS nanocomposites

2.3.1. ZnS core

The colloidal solution of ZnS is synthesized by injecting SH^- (2×10^{-4} mol dm^{-3}) to the respective degassed solution of $Zn(CH_3COO)_2$ (2×10^{-4} mol dm^{-3}) containing sodium hexametaphosphate (2×10^{-4} mol dm^{-3}) as stabilizer following the procedure as discussed earlier [25].

2.3.2. ZnS/PbS precursor

The colloidal solution of ZnS/PbS precursor was prepared by adding 100 μL of 0.1 mol dm^{-3} lead acetate (1.0×10^{-4} mol dm^{-3}) to the degassed solution of 100 ml colloidal solution of ZnS (2.0×10^{-4} mol dm^{-3}). This procedure results in the substitution of the surface Zn^{2+} ions by Pb^{2+} ions, forming a layer of PbS on ZnS. The PbS layer in this process is formed instantaneously because of several orders of magnitude lower solubility product of PbS (3.4×10^{-28}) compared to that of ZnS (1.2×10^{-23}) [34].

2.3.3. ZnS/PbS/ZnS nanocomposites

The ZnS/PbS precursor solution was treated with 1×10^{-4} mol dm^{-3} zinc acetate followed by injection of 1×10^{-4} mol dm^{-3} SH^- to form a ZnS layer in the outer shell of PbS. The resulting solution was subsequently purged with nitrogen. The pH of the solution was carefully maintained at 10.8 at every step of synthesis. The colloidal particles thus formed consisted of a ZnS core surrounded by a layer of PbS followed by a layer of ZnS as the outermost shell having ZnS and PbS at 1×10^{-4} mol dm^{-3} each (Scheme 1). The equivalent amount of ZnS shell to PbS has been considered corresponding to the first layer of ZnS.

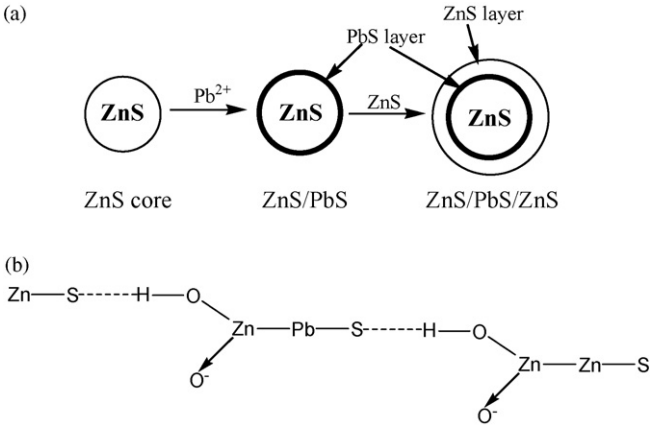

Scheme 1. (a) Formation of ZnS/PbS/ZnS nanoheterostructure. (b) Structure of ZnS/PbS/ZnS linked through $Zn(OH)_2$.

The thickness of the outer ZnS layer was increased by subsequent additions of Zn^{2+} (1×10^{-4}–5×10^{-4} mol dm^{-3}) followed by injection of the same amount of SH^-. After each addition the solution was purged with nitrogen to remove any excess H_2S.

3. Results and discussion

The absorption spectra of colloidal ZnS, precursor ZnS/PbS, and ZnS/PbS/ZnS layered nanoparticles as a function of increasing thickness of outer ZnS shell (1×10^{-4}–5×10^{-4} mol dm^{-3}) have been shown in Fig. 1A. An examination of these spectra reveals that the absorption due to ZnS/PbS/ZnS composites differs considerably from the sum of absorption due to two individual components ZnS/PbS and ZnS. An initial layer of ZnS shell results in a significant increase in the absorption of these composites below 420 nm and depicts a shoulder at 280 nm. ZnS is known to have an excitonic band at 280 nm (4.4 eV). It thus shows ZnS/PbS/ZnS nanolayered composite retains ZnS-based absorption. A subsequent increase in its thickness thereafter simply enhanced the absorption coefficient in the spectral range between 200 and 600 nm without causing any shift in the excitonic band.

The fluorescence spectra of the precursor ZnS/PbS and ZnS/PbS/ZnS nanocomposites obtained as a function of increasing concentration of outer ZnS layer have been presented in Fig. 1B. At low concentrations of the outer layer of ZnS (1×10^{-4} mol dm^{-3}), the excitation of ZnS/PbS/ZnS nanosystem by 295 nm (4.2 eV) light displays the bandgap emission centered at 505 nm (2.45 eV) (Fig. 1B), which is fairly blue shifted and is about 5-fold more intense (curve b) compared to that of ZnS/PbS precursor having a broad fluorescence band at 550 nm (2.25 eV) (curve a). An increase in the concentration of ZnS shell from 1×10^{-4} to 5×10^{-4} mol dm^{-3} gradually, red shifted the emission band accompanied with a reduction in its fluorescence intensity. A typical outer shell thickness corresponding to 5×10^{-4} mol dm^{-3} of ZnS red shifts the emission band to 530 nm (2.33 eV) associated with a reduction in its emission intensity by about 3.5-fold.

A stepwise addition of excess Zn^{2+} to colloidal ZnS/PbS/ZnS solution having the monolayer coverage of ZnS results in a slight increase in the absorption in the entire UV–vis region without causing any change in the excitonic peak (not shown). It though results in the enhancement of the emission intensity associated with slightly blue shifted emission maxima. An addition of 5×10^{-4} mol dm^{-3} of excess Zn^{2+} shifted the emission band from 2.45 to 2.5 eV and enhanced the intensity of this band by about 1.7-fold (inset: Fig. 1B).

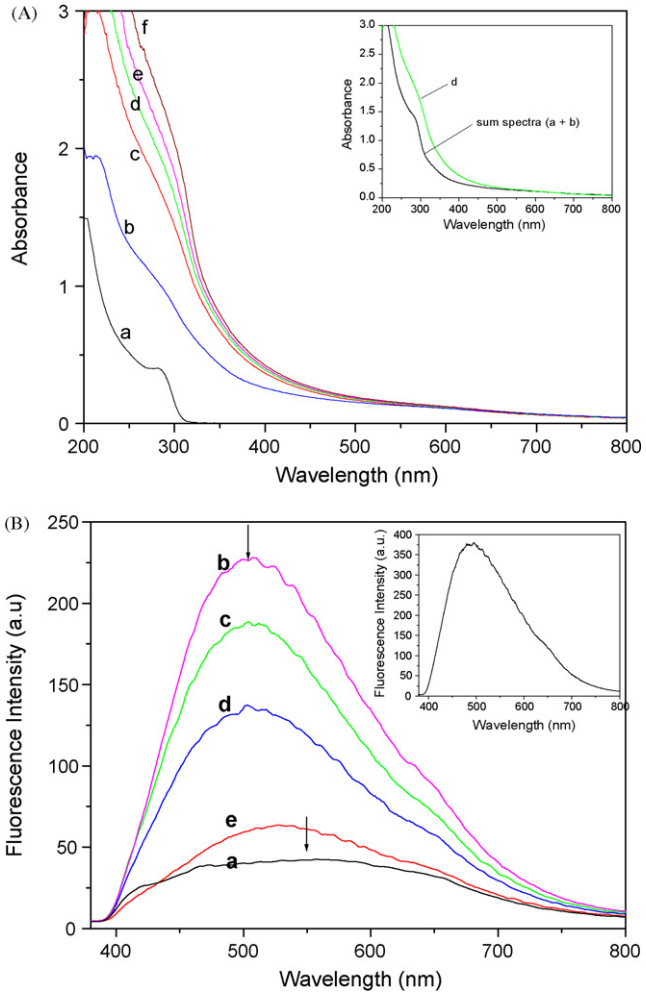

Fig. 1. (A) Electronic spectra of (a) ZnS (2×10^{-4} mol dm^{-3}); (b) ZnS/PbS (ZnS = 2×10^{-4} mol dm^{-3} + Pb^{2+} = 1×10^{-4} mol dm^{-3}); and ZnS/PbS in the presence of different amounts of outer shell of ZnS ($\times 10^{-4}$ mol dm^{-3})—1.0 (c); 2.0 (d); 3.0 (e); 5.0 (f); at pH 10.8. Inset: comparison of absorption spectra 'd' with the sum spectra of its individual components, i.e. 'a' and 'b'. (B) Emission spectra of precursor ZnS/PbS in the presence of different amounts of ZnS at its interface as shell ($\times 10^{-4}$ mol dm^{-3})—0.0 (a); 1.0 (b); 3.0 (c); 4.0 (d); 5.0 (e); at pH 10.8. λ_{ex} = 295 nm. Inset: emission spectra of ZnS/PbS/ZnS QDQW in the presence of extra Zn^{2+} (5×10^{-4} mol dm^{-3}).

The excitation of ZnS/PbS/ZnS particles containing 1×10^{-4} mol dm^{-3} ZnS in the outer layer by light of energy lower than 4.2 eV blue shifted the 505 nm bands along with a significant reduction in its emission intensity (Fig. 2A). A typical

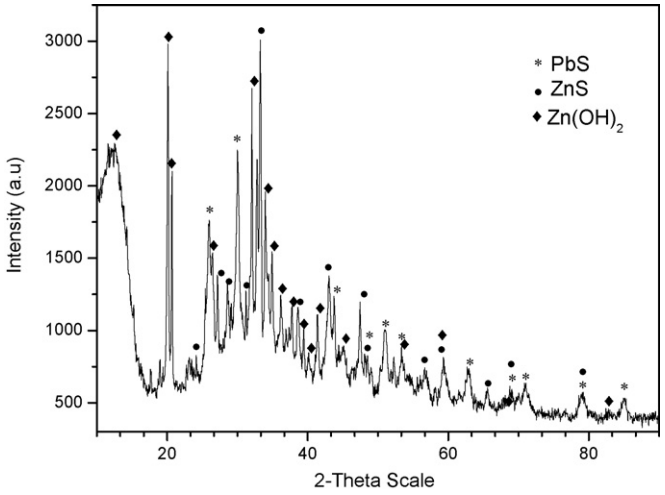

Fig. 3. X-ray diffraction patterns of ZnS/PbS/ZnS nanocomposites.

excitation of these particles by 380 nm (3.25 eV) radiation shifted the fluorescence maxima to 490 nm (2.5 eV) and reduced their fluorescence intensity by a factor of about 5.

X-ray diffraction (XRD) pattern of ZnS/PbS/ZnS composite with excess Zn^{2+} is shown in Fig. 3. A comparison of the values of d-spacing observed for ZnS/PbS/ZnS nanosystem with the literature data on bare ZnS and PbS [35] indicates that ZnS and PbS phases in the composite are present in wurtzite and face centered cubic structural forms, respectively (Table 1). The observed d-spacing also exhibits the presence of $Zn(OH)_2$ in orthorhombic form.

TEM images of bare colloidal PbS, ZnS, and ZnS/PbS/ZnS nanocomposites along with the SAED patterns of ZnS and ZnS/PbS/ZnS are depicted in Fig. 4. The electron micrograph of ZnS/PbS/ZnS nanocomposites exhibits the presence of aggregates consisting of mixed particles surrounding each other, which is supported by the observation made from XRD studies (Fig. 3). SAED patterns of ZnS/PbS/ZnS nanosystem also demonstrate the formation of rings corresponding to diffraction from planes: (1 0 2) and (2 0 0); and (2 0 0) and (4 0 0) of ZnS in wurtzite and PbS in fcc phases, respectively (Fig. 4E).

Relaxation kinetics of charge carriers in the precursor ZnS/PbS, ZnS/PbS/ZnS colloids covered by ZnS shell and the latter particles containing excess Zn^{2+} was followed upon their excitation by 295 nm radiation and monitoring the decay of the fluorescence kinetically at 505 nm. Some representative fluorescence lifetime decay curves obtained in the absence and presence of excess Zn^{2+} have been presented in Fig. 5. All decay curves could be best fitted in three-exponential kinetics consisting of three distinct time

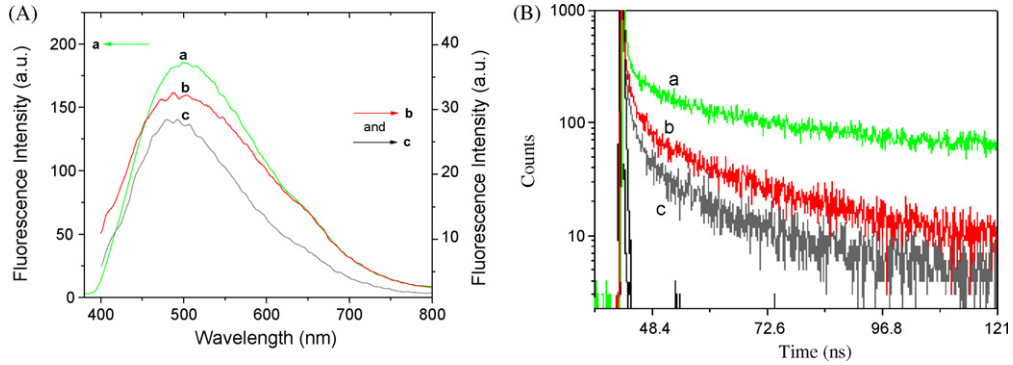

Fig. 2. (A) Emission spectra of ZnS/PbS/ZnS obtained under illumination excited with different excitation wavelengths λ_{ex} (nm) (a) 295; (b) 350; (c) 380 at pH 10.8. (B) Fluorescence decay curves of ZnS/PbS/ZnS QDQW using different excitation wavelengths (nm) (a) 295; (b) 380; (c) 405.

Table 1
A comparison of the observed '*d*' values (Å) in XRD pattern of mixed colloids (ZnS/PbS/ZnS) with the standard values of ZnS (wurtzite), PbS (face centered cubic), and $Zn(OH)_2$ (orthorhombic).

Observed value	Literature value		
	PbS (fcc)	ZnS (wurtzite)	$Zn(OH)_2$ (orthorhombic)
ZnS/PbS/ZnS			
4.38			4.38 (301)
4.28	4.27 (110)		
3.68			3.69 (305)
3.43	3.43 (111)		
3.32		3.31 (100)	
3.28		3.26 (102)	
3.12		3.13 (103)	
3.07		3.05 (104)	
2.97	2.97 (200)		
2.93		2.93 (105)	
2.85			2.85 (125)
2.77			2.77 (217)
2.72			2.71 (009)
2.62		2.61 (106)	
2.56			2.57 (020)
2.48		2.49 (107)	
2.45			2.45 (002)
2.32			2.32 (102)
2.28		2.27 (102)	
2.26			2.26 (021)
2.19			2.19 (220)
2.17			2.14 (112)
2.09	2.09 (220)		
1.91		1.91 (110)	
1.85			1.85 (302)
1.79	1.79 (311)		
1.76		1.76 (1015)	
1.75			1.74 (122)
1.71	1.71 (222)		
1.63			1.64 (420)
1.62		1.62 (112)	
1.58		1.57 (201)	
1.55		1.55 (004)	
1.47	1.48 (400)		
1.36	1.36 (331)		
1.32	1.32 (420)		
1.24		1.29 (203)	
1.21	1.21 (422)	1.21 (114)	
1.14	1.14 (511)		

range—the very fast, fast and relatively slow components lying in sub-nanosecond, nanosecond and microsecond range, respectively (Table 2). The formation of ZnS shell on ZnS/PbS precursor enhanced the lifetime enormously from 5.5 to 150 ns (Table 2a). A subsequent stepwise addition of excess Zn^{2+} (1×10^{-4}–5×10^{-4} mol dm^{-3}) to these colloidal solutions gradually enhanced $<\tau>$ from 150 to 250 ns (Table 2b). An examination of lifetime data in Table 2b reveals that although the lifetime of all the components is enhanced with increasing Zn^{2+} but for the component with longer time constants, it is increased significantly. In fact it is the longer lifetime component, which makes a major contribution (~90%) to the overall emission in comparison to the other two components upon addition of excess Zn^{2+}. A further increase in $[Zn^{2+}]$ coagulates this solution. From the values of τ of different components, the depths of different traps have been estimated to vary from 160 to 365 meV.

The composite particle ZnS/PbS/ZnS with primary layer of ZnS shell undergoes dissolution efficiently in the presence of O_2 under illumination by light >400 nm. The quantum efficiency of the photodissolution was determined by following the decomposition of colloids at various wavelengths and was estimated to be 0.04. In the presence of excess Zn^{2+} (4×10^{-4} mol dm^{-3}) the quantum efficiency of decomposition reduces significantly from 0.04 to 0.005.

The deposition of ZnS of varying thickness as shell at the interface of ZnS/PbS particles thus produces ZnS/PbS/ZnS nanocomposite in which PbS with a bulk bandgap of 0.41 eV is present in the well and is coated by ZnS shell having a bandgap of 3.2 eV similar to that required for the formation of QDQW (Scheme 1a) [28–31]. Remarkably, the average size of particles in ZnS/PbS/ZnS aggregates is about 7 nm, which is comparatively smaller to that of bare ZnS (av. dia. 10.5 nm) and similar to those of PbS (av. dia. 7 nm) prepared separately under identical conditions (Fig. 4). This indicates that ZnS produced at the interface of PbS particles is smaller and does not undergo agglomeration. X-ray diffraction studies demonstrate that ZnS/PbS/ZnS nanoheterostructure consists of PbS, ZnS and $Zn(OH)_2$ in face centered cubic, wurtzite and orthorhombic phases, respectively (Fig. 3). The formation of $Zn(OH)_2$ is understood by the presence of excess Zn^{2+} in this system in the basic medium (pH = 10.8) by taking in to account the literature pK_a value of 9.6 for Zn^{2+} hydrates [36]. These observations evidently suggest ZnS/PbS/ZnS composite to consist of quantum dot quantum well type nanoheterostructure, in which PbS colloids is sandwiched between layers of ZnS, and in the presence of excess Zn^{2+} at basic pH, PbS is attached to ZnS through $Zn(OH)_2$ as shown in Scheme 1b.

For these particles the observed red shift in the onset of absorption and a much higher absorption coefficient in the visible range between 350 and 500 nm, cannot simply be accounted for by this being the sum spectra of ZnS/PbS and added ZnS, as the sum spectra of the two species has less absorption in this range (inset: Fig. 1A). Moreover, ZnS does not have any absorption in the visible region, beyond 320 nm (3.88 eV). The emission spectra of ZnS/PbS/ZnS composites depict a broad fluorescence band at 505 nm, which is quite different from pure ZnS or precursor ZnS/PbS particles, having emission bands at 460 nm (2.7 eV) and 550 nm (2.25 eV), respectively. It is remarkable that a change in absorption behavior is more prominent by the formation of the first layer of ZnS and becomes relatively less significant by the deposition of subsequent layers. Similar changes are seen in the emission studies in which the deposition of the first layer brings about 5-fold increase in the intensity of emission associated with a blue-shift in the fluorescence peak (Fig. 1B) followed by a decrease in emission intensity by the deposition of subsequent layers. These changes clearly suggest relatively higher interaction of the primary layer of ZnS with ZnS/PbS precursor. The subsequent layers simply passivate the surface in a different manner possibly by creating more defects. PbS thus forms a quantum well and is sandwiched between the layers of ZnS. The addition of excess Zn^{2+} ions may simply create additional traps involved in radiative recombination. The excess Zn^{2+}, present as $Zn(OH)_2$ at pH 10.8 might also passivate the surface of ZnS/PbS/ZnS to enhance the radiative recombination. The participation of $Zn(OH)_2$ to cause an increase in the quantum efficiency of emission has earlier been observed for RNA-mediated Q-PbS [37] and DNA-mediated colloidal Q-CdS particles [38]. Another possibility that $Zn(OH)_2$ itself might contribute to the emission around 500 nm was examined in a control experiment by recording the emission spectra of $Zn(OH)_2$ [39]. It exhibits negligibly small emission around 500 nm and thus rules out its contribution to the observed emission.

A substantial increase in absorption due to ZnS/PbS/ZnS nanoheterostructure below 500 nm compared to the sum spectra of two individual components (inset: Fig. 1) associated with significantly higher change in emission reflects increased oscillator strength of optical transition(s) involved in this system. It might have arisen due to higher density of charge carriers confined in the core–shell structure, which may also result in enhanced radiative recombination. A strong interfacial interaction between ZnS/PbS and ZnS moieties is also supported by a tremendous increase in the emission lifetime from 5.5 to 150 ns by the formation of a ZnS shell on precursor ZnS/PbS (Fig. 5 and Table 2a). It may be pointed out that these lifetimes are significantly different from the lifetime of precursor namely ZnS [27] and ZnS/PbS, respectively both of which

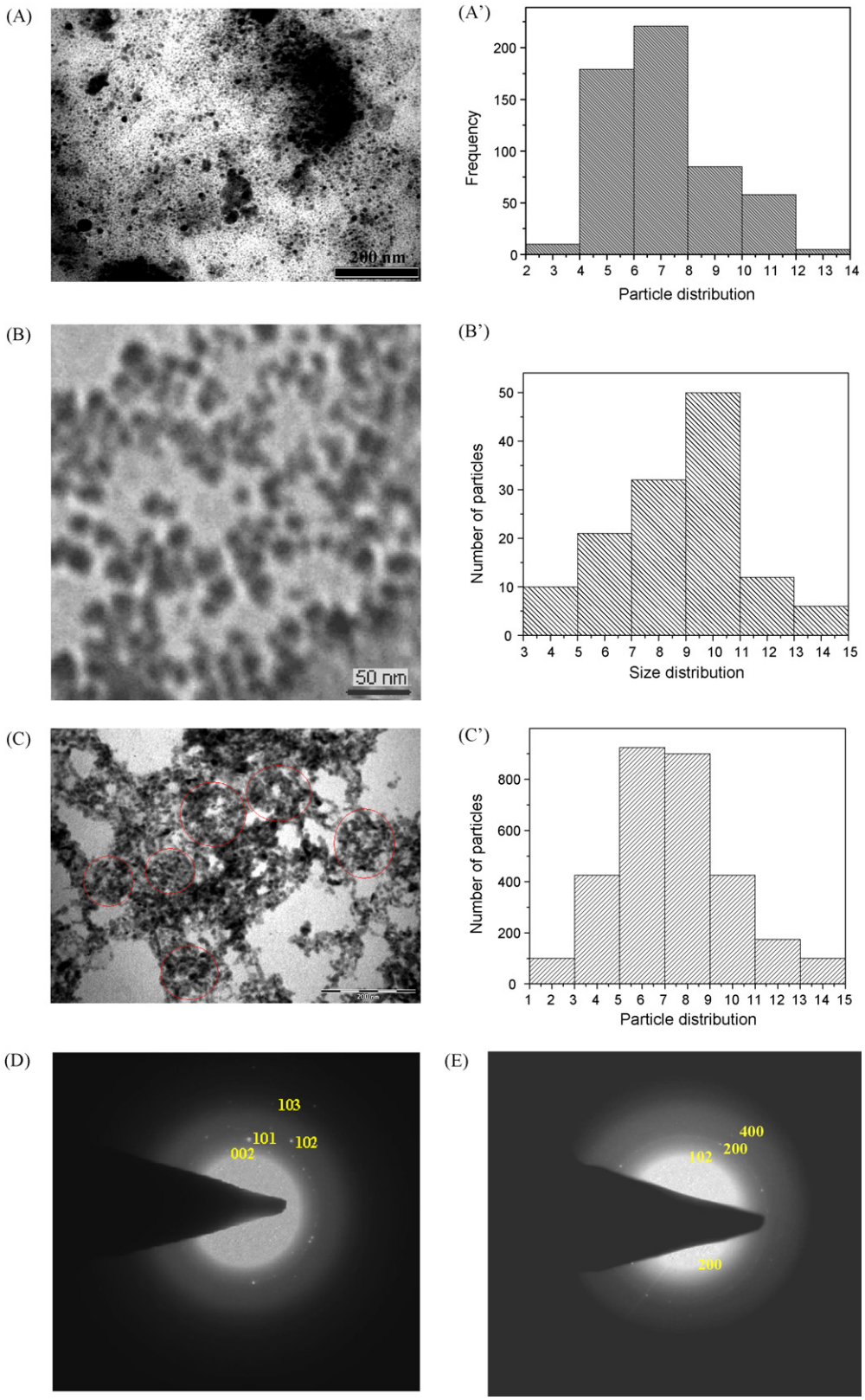

Fig. 4. Electron micrograph(s) and size histograms of colloidal PbS (A and A′); ZnS (B and B′); ZnS/PbS/ZnS (C and C′) nanoparticles. SAED patterns of nanoparticles shown electron micrographs B (D) and C (E).

lie in the nanosecond time domain (Table 2). Thus the monolayer coverage of ZnS passivates the surface vacancies lying in the shallow traps of these composites and thereby enhances the radiative recombination.

The fact that emission could be observed upon excitation of these composites by low energy photons (3.25 eV), which are not absorbed by ZnS phase, it evidently manifests that emission has not originated from ZnS center. The possibility of emission

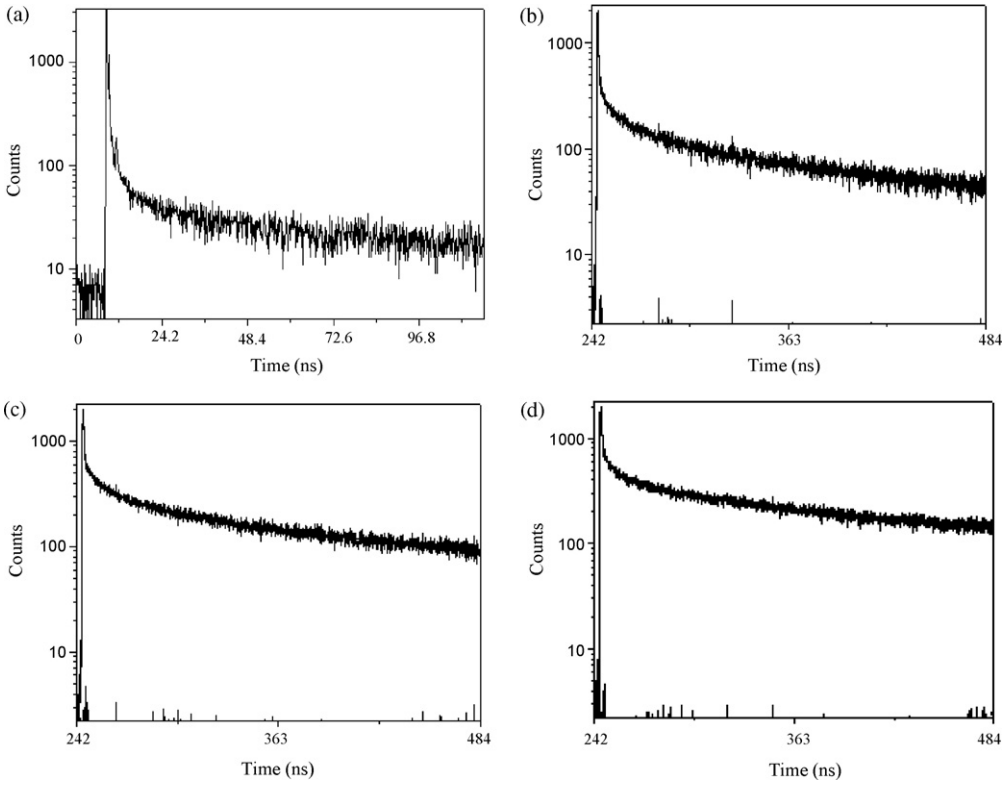

Fig. 5. Fluorescence decay curves of precursor ZnS/PbS (a) (time calibration = 5.095×10^{-11} s/channel) and ZnS/PbS/ZnS containing different amounts of Zn^{2+} ($\times 10^{-4}$ mol dm^{-3}): 0.0 (b); 1.0 (c); 5.0 (d) λ_{ex} = 295 nm; λ_{em} = 505 nm at pH 10.8. Time calibration = 1.21×10^{-10} s/channel.

from PbS phase alone is also ruled out as colloidal PbS stabilized by HMP depicts negligible emission in the recorded wavelength range. Thus the observed emission does not arise from either of ZnS and PbS phase alone instead it is contributed by the entire ZnS/PbS/ZnS nanocomposite in a complex mechanism (Scheme 2). It is likely that the binding of ZnS and PbS phases through $Zn(OH)_2$ (Scheme 1B) modifies their energy levels such that it facilitates the transfer of hole from PbS to ZnS phase. The transfer of hole is supported by the observed decrease in fluorescence intensity (Fig. 2A) associated with a decrease in emission lifetime upon excitation of these particles by low energy photons (Table 2c). This aspect though needs further elaborate investigation. Even more significant observations about the excitation of these particles by lower energy radiation is that it blue shifts the emission maxima which decays rapidly compared to observed upon excitation by 295 nm, suggesting the involvements of shal-

Table 2
Fluorescence lifetime data at pH 10.8.

Lifetime (ns)								
System	Component 1		Component 2		Component 3		<τ>(ns)	χ^2
	τ_1	Emission %	τ_2	Emission %	τ_3	Emission %		
(a) Lifetime of mixed ZnS/PbS precursor and ZnS/PbS/ZnS composite; λ_{ex} = 295 nm; λ_{em} = 505 nm								
ZnS/PbS precursor	0.0665 (0.44)	41.61	1.15 (0.01)	15.52	12.4 (0.002)	2.87	5.5	1.2
ZnS/PbS/ZnS QDQW	0.152 (1.14)	9.11	13.2 (0.015)	10.40	184 (0.008)	80.49	150	1.1
Zn^{2+} (mol dm^{-3})	Component 1		Component 2		Component 3		<τ>(ns)	χ^2
	τ_1	Emission %	τ_2	Emission %	τ_3	Emission %		
(b) Effect of addition of Zn^{2+} on the lifetime of mixed ZnS/PbS/ZnS composites; λ_{ex} = 295 nm; λ_{em} = 505 nm								
0	0.152 (1.14)	9.11	13.2 (0.015)	10.40	184 (0.008)	80.49	150	1.1
1×10^{-4}	0.23 (0.63)	3.58	16.8 (0.021)	8.91	228 (0.015)	87.51	210	1.2
3×10^{-4}	0.337 (0.41)	2.32	13.4 (0.023)	5.31	252 (0.021)	92.38	230	1.2
5×10^{-4}	0.351 (0.39)	2.09	15.5 (0.021)	5.07	271 (0.022)	92.84	250	1.2
λ_{ex} (nm)	Component 1		Component 2		Component 3		<τ>(ns)	χ^2
	τ_1	Emission %	τ_2	Emission %	τ_3	Emission %		
(c) Effect of the excitation energy on lifetime of ZnS/PbS/ZnS composites λ_{em} = 505 nm								
295	0.152 (1.14)	9.11	13.2 (0.015)	10.40	184 (0.008)	80.49	150	1.1
380	0.333 (1.05)	26.19	3.03 (0.096)	21.73	38.4 (0.018)	52.07	21	1.1
405	0.227 (1.65)	39.84	2.17 (0.114)	26.44	26.6 (0.019)	33.71	10	1.2

Values in bracket are pre-exponential factor corresponding to respective τ.

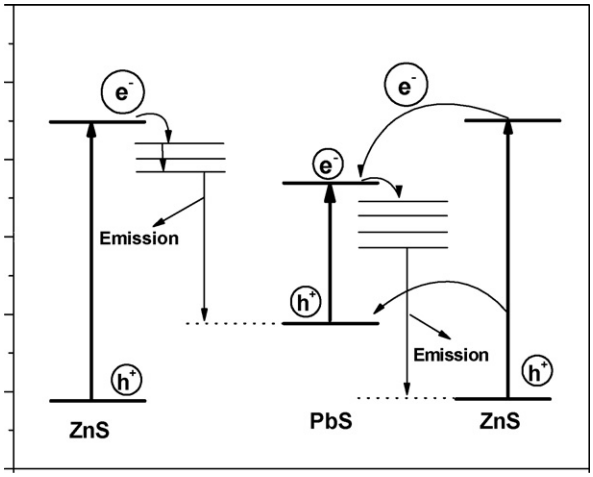

Scheme 2. Energy level diagram depicting photophysical changes in ZnS/PbS/ZnS nanocomposites.

low traps present at the interface in the process at lower energy (Fig. 2).

In ZnS/PbS/ZnS nanocomposites, ZnS and PbS being present in wurtzite (a = 3.82 Å, c = 6.26 Å) and face centered cubic form (a = 5.9362 Å) have a mismatch in lattice constants. Even in the crystal surface 'c' of ZnS, it is higher by 5.45% to that of PbS. Since the precursor ZnS/PbS and outer shell ZnS being nanocolloids contribute large interface, the lattice mismatch between the two may create surface states of varied energy acting as traps for charge carriers. Relaxation kinetics clearly demonstrates a distribution of traps of varied energy ranging from 160 to 365 meV on the entire surface (Fig. 2B and Table 2c). It is also manifested by a significant reduction in $<\tau>$ from 150 to 21 ns by a decrease in excitation energy from 4.2 to 3.25 eV. Since neither of ZnS, PbS and ZnS/PbS phases alone can demonstrate the above observed absorption and emission characteristics, obviously, the presence of PbS in the well of ZnS/PbS/ZnS provides an interface, which results in the confinement of charge carriers in traps of varied energy and thus manipulate the electronic levels to exhibit these features.

4. Summary

In summary the formation of monolayer of ZnS at the interface of ZnS/PbS precursor results in the formation of ZnS/PbS/ZnS nanoheterostructure containing PbS in the well with significantly improved fluorescence. A lattice mismatch between the two nanocolloids creates a large interface in which the surface states of varied energy are generated. The monolayer of ZnS shell enhances the oscillator strength of optical transition in the core–shell structure due to increase in quantum confinement of charge carriers and radiative recombination in shallow traps, whereas the formation of multilayer induces the radiative recombination involving mainly deeper traps. An energy dependence decay of fluorescence in these particles suggests the delocalization of traps on the entire surface. The addition of excess Zn^{2+} to these particles enhances their photostability and improves the charge separation. As prepared ZnS/PbS/ZnS nanocomposite has different nanodomains in which electronic interactions and the charge dynamics could be manipulated by exciting the nanocomposite as a whole. Manipulation of electronic properties in these systems can be exploited for the fabrication of optoelectronic devices and designing of fluorescent sensors. Such a system might be encountered in galena-sphalerite mixed sulfide ore occurring in nature consisting of excess ZnS and little PbS [40].

Acknowledgments

The financial support of DST, New Delhi is gratefully acknowledged in undertaking this work. AJ and VC are thankful to CSIR, New Delhi and MHRD, New Delhi, respectively for the award of SRF. Thanks are also due to the Director, AIIMS, New Delhi and Head, IIC, IIT Roorkee for providing us with TEM and single photon counting facilities, respectively and Mr. Bhupendra Singh for help in some experiments in revising the MS.

References

[1] J. Fick, A. Martucci, Lead sulfide nanoparticles, in: H.S. Nalwa (Ed.), Encyclopedia of Nanoscience and Nanotechnology, vol. 4, American Scientific Publishers, Stevenson Ranch, CA, 2004, pp. 481–504.
[2] S.A. Mcdonald, G. Konstantatos, S. Zhang, P.W. Cyr, E.J.D. Klem, L. Levina, E.H. Sargent, Solution-processed PbS quantum dot infrared photodetectors and photovoltaics, Nat. Mater. 4 (2005) 138–142.
[3] M.A. Hines, G.D. Scholes, Colloidal PbS nanocrystals with size-tunable near-infrared emission: observation of post-synthesis self-narrowing of the particle size distribution, Adv. Mater. 15 (2003) 1844–1849.
[4] L. Guo, X.C. Ai, Femtosecond optical Kerr effect of PbS nanoparticles modification effect, Mater. Chem. Phys. 63 (2000) 30–36.
[5] E.H. Sargent, Infrared quantum dots, Adv. Mater. 17 (2005) 515–522.
[6] A.L. Rogach, A. Eychmüller, S.G. Hickey, S.V. Kershaw, Infrared emitting colloidal nanocrystals: synthesis, assembly, spectroscopy and applications, Small 3 (2007) 536–557.
[7] Y. Yang, M. Nogami, J. Shi, H. Chen, Y. Liu, S. Qian, Self-assembled semiconductor capped metal composite nanoparticles embedded in $BaTiO_3$ thin films for nonlinear optical applications, J. Mater. Chem. 13 (2003) 3026–3032.
[8] S.W. Lu, U. Sohling, M. Menning, H. Schmidt, Nonlinear optical properties of lead sulfide nanocrystals in polymeric coatings, Nanotechnology 13 (2002) 669–673.
[9] F.W. Wise, Lead salt quantum dots: the limits of strong quantum confinement, Acc. Chem. Res. 33 (2000) 773–780.
[10] A.P. Alivisatos, The use of nanocrystals in biological detection, Nat. Biotechnol. 22 (2004) 47–52.
[11] C. Zhang, Z. Kang, E. Shen, E. Wang, L. Gao, F. Luo, C. Tian, C. Wang, Y. Lan, J. Li, X. Cao, Synthesis and evolution of PbS nanocrystals through a surfactant-assisted solvothermal route, J. Phys. Chem. B 110 (2006) 184–189.
[12] S. Yang, S. Wang, K.K. Fung, One-dimensional growth of rock-salt PbS nanocrystals mediated by surfactant/polymer templates, Pure Appl. Chem. 72 (2000) 119–126.
[13] S. Wang, S. Yang, Preparation and characterization of oriented PbS crystalline nanorods in polymer films, Langmuir 16 (2000) 389–397.
[14] T. Cui, F. Cui, J. Zhang, J. Wang, J. Huang, C. Lü, Z. Chen, B. Yang, From monomeric nanofibres to PbS nanoparticles/polymer composite nanofibres through the combined use of γ-irradiation and gas/solid reaction, J. Am. Chem. Soc. 128 (2006) 6298–6299.
[15] N. Pellegri, R. Trbojevich, O.D. Sanctis, K. Kadono, Fabrication of PbS nanoparticles embedded in silica gel by reverse micelles and sol–gel routes, J. Sol–Gel Sci. Technol. 8 (1997) 1023–1028.
[16] J. Eastoe, A.R. Cox, Formation of PbS nanoclusters using reverse micelles of lead and sodium aerosol-OT, Colloids Surf. A: Physicochem. Eng. Aspects 101 (1995) 63–76.
[17] S. Wu, H. Zeng, Z.A. Schelly, Preparation of ultrasmall, uncapped PbS quantum dots via electroporation of vesicles, Langmuir 21 (2005) 686–691.
[18] M. Wark, N.I. Jaeger, W. Lutz, O.P. Tkachenko, Influence of the zeolite matrix on the optical properties and the stability of hosted PbS nanoparticles, Ber. Bunsenges. Phys. Chem. 101 (1997) 1635–1640.
[19] C. Leiggener, G. Calzaferri, Synthesis and luminescence properties of Ag_2S and PbS clusters in zeolite A, Chem. Eur. J. 11 (2005) 7191–7198.
[20] Y.N. Savin, S.V. Vitushkina, PbS nanoparticles in Langmuir–Blodgett films: kinetics of formation and growth, Phys. Stat. Sol. B 241 (2004) 1026–1031.
[21] A.A. Lipovskii, E.V. Kolobkova, A. Olkhovets, V.D. Petrikov, F. Wise, Synthesis of monodisperse PbS quantum dots in phosphate glass, Physica E 5 (2000) 157–160.
[22] T. Okuno, A.A. Lipovskii, T. Ogawa, I. Amagai, Y. Masumoto, Strong confinement of PbSe and PbS quantum dots, J. Lumin. 87 (2000) 491–493.
[23] P.H.C. Camargo, Y.H. Lee, U. Jeong, Z. Zou, Y. Xia, Cation exchange: a simple and versatile route to inorganic colloidal spheres with the same size but different compositions and properties, Langmuir 23 (2007) 2985–2992.
[24] D.H. Son, S.M. Hughes, Y. Yin, A.P. Alivisatos, Cation exchange reactions in ionic nanocrystals, Science 306 (2004) 1009–1012.
[25] A.P. Alivisatos, Perspectives on the physical chemistry of semiconductor nanocrystals, J. Phys. Chem. 100 (1996) 13226–13239.
[26] A. Kumar, Physicochemical and photochemical properties of nanoscale semiconductors—dynamics of the charge carriers, Natl. Acad. Sci. Lett. 28 (2005) 1–11.
[27] A. Kumar, A. Jakhmola, Photophysics and charge dynamics of Q-PbS based mixed ZnS/PbS and PbS/ZnS semiconductor nanoparticles, J. Colloid Interface Sci. 297 (2006) 607–617.

[28] R.B. Little, M.A. El-Sayed, G.W. Bryant, S. Burke, Formation of quantum-dot quantum well heterostructures with large lattice mismatch: ZnS/CdS/ZnS, J. Chem. Phys. 114 (2001) 1813–1822.
[29] G.W. Bryant, W. Jaskólski, Designing nanocrystal nanosystems: quantum-dot quantum-wells to quantum-dot solids, Phys. Stat. Sol. B 224 (2001) 751–755.
[30] E. Lifshitz, H. Porteanu, A. Glozman, H. Weller, M. Pflughoefft, A. Echymüller, Optically detected magnetic resonance study of CdS/HgS/CdS quantum dot quantum wells, J. Phys. Chem. B 103 (1999) 6870–6875.
[31] Y. Li, J. Feng, S. Daniels, N.L. Pickett, P. O'Brien, A highly luminescent ZnS/CdSe/ZnS nanocrystals-tetrapeptide biolabeling agent, J. Nanosci. Nanotechnol. 7 (2007) 2301–2308.
[32] D.R. James, Y.–S. Liu, P. de Mayo, W.R. Ware, Distributions of fluorescence lifetimes. Consequences for the photophysics of molecules adsorbed on surfaces, Chem. Phys. Lett. 120 (1985) 460–465.
[33] A. Eychmüller, A. Hässelbarth, L. Katsikas, H. Weller, Fluorescence mechanism of highly monodisperse Q-sized CdS colloids, J. Lumin. 48–49 (1991) 745–749.
[34] R.C. Weast (Ed.), Handbook of Chemistry and Physics, CRC, Boca Raton, FL, 1978, p. B-254.
[35] Joint committee on powder diffraction standards, Inorganic index to the powder diffraction file, International center of diffraction data, USA, 1971, pp. 380, 627, 638, 641, 645, 683.
[36] J. Ciesiolka, D. Michalowski, J. Wrzesinski, J. Krajewski, W.J. Krzyzosiak, Patterns of cleavages induced by lead ions in defined RNA secondary structure motifs, J. Mol. Biol. 275 (1998) 211–220.
[37] A. Kumar, A. Jakhmola, RNA-templated fluorescent Zn/PbS (PbS + Zn^{2+}) supernanostructures, J. Phys. Chem. C 113 (2009) 9553–9559.
[38] S.R. Bigham, J.L. Coffer, Deactivation of Q-CdS photoluminescence through polynucleotide surface binding, J. Phys. Chem. 96 (1992) 10581–10584.
[39] In a control experiment, the emission spectra of aqueous Zn^{2+} solution (1×10^{-4} to 5×10^{-4} mol dm^{-3}) at pH 10.8 were recorded by excitation of these samples by 295 nm light. It exhibits negligibly small emission around 500 nm which rules out the possibility of $Zn(OH)_2$ contributing to the process.
[40] J. Park, Distribution of ores in horizontal zones in vertical depth, Trans. Proc. R. Soc. New Zeal. 39 (1906) 90–92.